F. Janssens
Mathematical Support Division, ESA Technical Directorate, ESTEC, Noordwijk, The Netherlands

Mathematical Modelling of a Flexible Beam under Gravity

Abstract The differential equations describing the static deflections of a Bernouilli beam under gravity and a concentrated tip load are derived and solved. The solutions are used to predict tip deflections as a function of bending stiffness for a constant tip load. This relationship is then applied to the results of the static bending tests performed on the ISPM satellite's axial antenna to determine its bending stiffness. The results show clearly the importance of modelling gravity as a distributed load, even for light structural elements.

Résumé Cet article établit et résout les équations différentielles auxquelles obéit la flexion statique produite par l'action de la pesanteur sur une poutre conforme à la loi de Bernouilli avec charge concentrée aux extrémités.

A partir des solutions trouvées, on calcule les flexions d'extrémité en fonction de la rigidité à la flexion pour une charge en bout constante. On applique ensuite la relation aux résultats des essais de flexion statique effectués sur l'antenne axiale de la sonde ISPM enfin de déterminer sa rigidité à la flexion. Les résultats montrent clairement l'importance d'une modélisation de la pesanteur en tant que charge répartie, même pour les éléments de structure de faible poids.

Introduction

The increasing size and flexibility of appendages on modern spacecraft introduces a particular problem when these elements are tested under normal gravity. In spite of their small mass, the dimensions of these appendages are often such that the distributed load due to gravity cannot be neglected in full-scale tests. The equations used to interpret the measurements of such a full-scale test must include this effect.

A simple, but typical example is the axial antenna to be flown on the Agency's International Solar-Polar Mission (ISPM) satellite. This newly developed antenna (by Sener) is up to 8 m long and has a mass of 272 g. It is stowed on a drum during launch in an elastically pre-stressed state, and it is then flat in cross-section. Following deployment, it assumes a double symmetric shape due to the prestressing and the two ensuing principal bending directions have different stiffnesses. It is a requirement that the minimum bending stiffness should exceed $16\,\mathrm{Nm}^2$.

A first measurement of bending stiffness was performed with the antenna floating on water, thus compensating for gravity effects. The bending stiffness could then be obtained directly from the lateral deflections due to a tip load. However, due to the nature of the floatation devices, it was possible to perform these tests only for the two principal bending directions. Furthermore, the floatation devices tended to remove any natural pretwisting of the beam about its axis.

To verify the earlier results and measure the deflections for different bending directions, it was decided to measure the tip deflections with the antenna hanging vertically, clamped at the top (deployment unit) and free at its lower end, where a horizontal force was applied and the deformation measured.

The aim of this paper is to derive and solve the equations describing the behaviour of such a beam. Assuming small deflections, these equations become linear, with variable coefficients of the polynomial type, and a complete set of base solutions can be generated from the corresponding recurrence relation. The predictions for the deflections based on this model are in agreement with the results of the previous tests. Other approaches, in which the distributed load due to gravity is replaced by an 'equivalent' concentrated load at the tip, produce results that are in error by an order of magnitude.

Bending equations for slender beams

A set of general vectorial equations describing the bending deflections of Bernouilli beams are first considered and used as the common starting point for problem analysis. These general equations are derived under all the well-known assumptions that define the slender Bernouilli beam[1,2]. In particular, inner moments and forces are defined which average the stresses over a cross-section. The rotational inertia of a cross-section is neglected, as well as the shear deformation, and the beam is considered inextensible. These assumptions are valid for the problem considered here. The general equations allow the treatment of static and dynamic three-dimensional deflections which are geometrically non-linear (they are discussed in more detail in Reference 3). They are applied to the following cases:

(i) A straight beam hanging under gravity, clamped at its root and subjected to a horizontal concentrated tip load along a principal bending direction.
(ii) The same as (i), with an arbitrary direction for the concentrated load.
(iii) Vibrations of (i) in the absence of the concentrated load.

General equations

The first equation is Newton's second law of motion applied to a beam element ds under the influence of the inner force and moment $-\bar{F}(s)$, $-\bar{M}(s)$ acting on the cross-section at s, the inner force and moment $\bar{F}(s+\mathrm{d}s)$, $\bar{M}(s+\mathrm{d}s)$ acting on the cross-section at $s+\mathrm{d}s$ and the resultants $\bar{F}_a$, $\bar{M}_a$ of the remaining applied forces (concentrated or distributed):

$$-\frac{\partial \bar{F}}{\partial s} + \mu \frac{d^2 \bar{R}}{dt^2} = \bar{F}_a \tag{1}$$

In slender-beam theory, $\bar{F}(s,t)$, $\bar{M}(s,t)$ summarise the stresses in the cross-sections. They are called the inner force and couple and are part of the response of the system to $\bar{F}_a$, $\bar{M}_a$. They appear, accordingly, in the left-hand side of Equation 1. The inertia term contains the linear density μ, the position vector $\bar{R}(s,t)$ from an inertial origin to the material point at s of the centre line, and d/dt, the rate of change as seen from inertial space.

Taking moments about the point $s + ds$, while neglecting the rotary inertia of the beam element ds, we obtain the second equation

$$-\frac{\partial \bar{M}}{\partial s} - \frac{\partial \bar{R}}{\partial s} \times \bar{F} = \bar{M}_a \tag{2}$$

The cross product in the unknowns $\bar{R}$ and $\bar{F}$ makes Equation 2 nonlinear. Equations 1 and 2 are also given in Reference 2. They are better known in more specialised forms (no vector equations) that describe planar deformations.

The next equation is an expression of Hookes' law and relates the inner moment $\bar{M}$ to the curvature $\bar{\kappa}$ via the elastic properties of the cross-section:

$$\bar{M} = TST^T(\bar{\kappa} - \bar{\kappa}_0) \tag{3}$$

where $\bar{\kappa}_0$ is the natural curvature corresponding to a stress-free state. S is the matrix representation of a second-order symmetric tensor which summarises the elastic properties of the cross section in the so-called 'Principal Flexural-Torsional axis system ('PFT system)[1], where it takes a diagonal form for a double symmetric cross-section. The PFT system at s carries a unit vector tangent to the centre line in the increasing sense of s, and two unit vectors perpendicular to the centre line and along the principal bending directions:

$$S = \begin{bmatrix} EI_x & 0 & 0 \\ 0 & EI_y & 0 \\ 0 & 0 & GA \end{bmatrix} \tag{4}$$

where EI_x, EI_y are principal bending stiffnesses, and GA is the torsional stiffness.

T is a rotation matrix between the PFT system and a chosen reference frame. The matrix expression TST^T represents the elastic tensor in the (arbitrarily) chosen reference frame. The physical content of Equation 3 is base-independent, which is reflected by the vectors $\bar{M}$, $\bar{\kappa}$, $\bar{\kappa}_0$ and the matrix notation TST^T for the second-order tensor.

The assumptions of inextensibility of the beam and the neglecting of the shear deformations eliminate a second equation of the same type between the inner forces and longitudinal deformations[3]. In the terminology of Reference 4, Equations 1 and 2 are balance equations and Equation 3 is a constitutive equation.

The three equations presented so far are equivalent to 9 scalar equations and contain the 12 unknowns from the components of $\bar{F}$, $\bar{R}$, $\bar{M}$, $\bar{\kappa}$ (derivatives do not introduce new unknowns) and the three unknowns defining T when T is an s-dependent matrix. The three unknowns of T are equivalent to the three components of a rotation vector $\bar{\theta}$:

$$\bar{\theta} = \theta \bar{1}_\theta = [\theta_1\ \theta_2\ \theta_3]^T \tag{5}$$

where θ is the magnitude of the rotation and $\bar{1}_\theta$ a unit vector on the rotation axis. The general nonlinear relation between the curvature $\bar{\kappa}$ and this rotation vector is[3]:

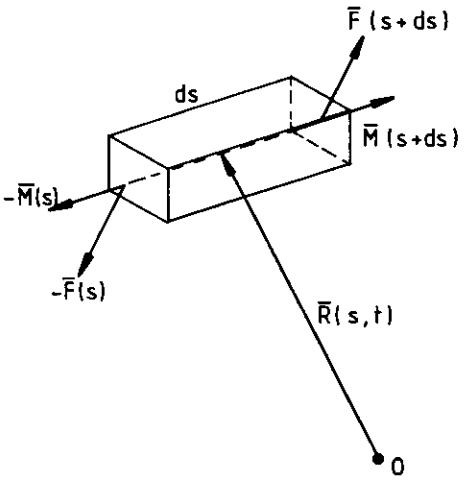

Figure 1. Equilibrium of a beam element.

$$\bar{\kappa} = \frac{d\theta}{ds}\bar{l}_\theta + \sin\theta\frac{d}{ds}(\bar{l}_\theta) + 2\sin^2\frac{\theta}{2}\left[\bar{l}_\theta \times \frac{d}{ds}(\bar{l}_\theta)\right] \tag{6}$$

Note that Equation 6 reduces to

$$\bar{\kappa} = \frac{d}{ds}\bar{\theta} \tag{7}$$

when $\bar{\theta}$ has a constant direction $[(d/ds)(\bar{l}_\theta) = 0]$ or when $\bar{\theta}$ is small and second-order terms are neglected. Only this form will be used in this paper.

We now have 12 equations for 15 unknowns and the last vector equation (essentially contained in Ref. 1 in component form) is

$$\frac{d}{ds}\bar{R} = T\,\bar{l} \tag{8}$$

which gives the expression for the tangent to the centre line in the chosen reference frame, $d\bar{R}/ds$ (containing the unknowns of $\bar{R}$) as the transformation via T (unknowns θ_i) of $\bar{l} = [001]^T$ (PFT system).

Equations 1, 2, 3, 7 and 8 constitute the complete set of general equations. For the static deflections of a naturally straight, flexible beam, hanging under gravity and subjected to a concentrated load at the tip, Equations 1–3 become:

$$-\frac{\partial\bar{F}}{\partial s} = \mu g\,\bar{l}_z \tag{9}$$

$$-\frac{\partial\bar{M}}{\partial s} - \frac{\partial\bar{R}}{\partial s} \times \bar{F} = 0 \tag{10}$$

$$\bar{M} = T\,S\,T^T\bar{\kappa} \tag{11}$$

where g is the gravitational acceleration and $\bar{l}_z$ the unit vector along the gravitational acceleration.

It should be noted that the tip force $\bar{F}_T$ is used as a boundary condition in the equations of motion.

The same dextral reference frame will be used for all the cases mentioned at the beginning of this section. The root of the beam is the origin and the beam is clamped at this point (Fig.2). The z-axis is vertical and oriented downwards. The x- and y-axes are horizontal and contain the principal bending directions of the cross-section at the root.

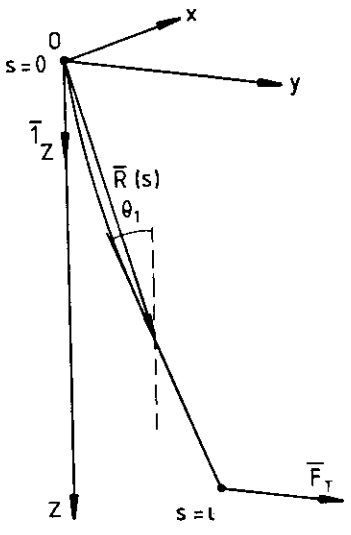

Figure 2. Axis system for beam deflections

Planar static deflections

We consider first the case when the applied load is horizontal and parallel to the y-axis. The deflections will be in the z,y-plane but, at this level, they are not restricted to small deflections. We denote the components of the vectors in the $0xyz$ frame as follows:

$$\bar{F}(s) = [F_x\,F_y\,F_z]^T \quad \bar{M}(s) = [M_x\,M_y\,M_z]^T \quad \bar{\kappa} = [\kappa_x\,\kappa_y\,\kappa_z]^T$$

$$\bar{F}_a = [0\,0\,\mu g]^T \qquad \bar{\theta}(s) = [\theta_1\,0\,0] \qquad \bar{F}_T = [0\,F_T\,0]^T$$

The matrix T is, in this case, a single axis rotation about the fixed x-direction:

$$T = \begin{bmatrix} 1 & 0 & 0 \\ 0 & \cos\theta_1 & -\sin\theta_1 \\ 0 & \sin\theta_1 & \cos\theta_1 \end{bmatrix} \tag{12}$$

Equation 9 leads to:

$$-F_x' = 0 \qquad -F_y' = 0 \qquad -F_z' = \mu g \qquad \left[(\ )' = \frac{d(\ )}{ds} \right]$$

which are trivial. The constants of integration follow from the boundary condition at the tip. We obtain, after integration,

$$F_x(s) = 0 \qquad F_y(s) = F_T \qquad F_z(s) = \mu g (l - s) \tag{13}$$

In Equation 10 we use the expression for $d\bar{R}/ds$ that takes the compatibility Equation 8 into account:

$$\frac{d\bar{R}}{ds} = \begin{bmatrix} \frac{dx}{ds} \\ \frac{dy}{ds} \\ \frac{dz}{ds} \end{bmatrix} = T\bar{1} = \begin{bmatrix} 1 & 0 & 0 \\ 0 & \cos\theta_1 & -\sin\theta_1 \\ 0 & \sin\theta_1 & \cos\theta_1 \end{bmatrix} \begin{bmatrix} 0 \\ 0 \\ 1 \end{bmatrix} = \begin{bmatrix} 0 \\ -\sin\theta_1 \\ \cos\theta_1 \end{bmatrix}$$

from which $\frac{d\bar{R}}{ds} = [0 \quad -\sin\theta_1 \quad \cos\theta_1]^T$

The components of Equation 10 are calculated as

$$-M_x' + \sin\theta_1 \, \mu g (l - s) + F_T \cos\theta_1 = 0 \qquad M_y' = 0 \qquad M_z' = 0 \tag{14}$$

and give a nontrivial equation only for the M_x component, as expected. As $\bar{\kappa}$ contains also only one nonzero component (from Equation 7), $\kappa_1 = \theta_1'$, we need Equation 11 only for the relation between M_x and θ_1:

$$\begin{bmatrix} M_x \\ 0 \\ 0 \end{bmatrix} = \begin{bmatrix} 1 & 0 & 0 \\ 0 & \cos\theta_1 & -\sin\theta_1 \\ 0 & \sin\theta_1 & \cos\theta_1 \end{bmatrix} \begin{bmatrix} EI_x & & \\ & EI_y & \\ & & GA \end{bmatrix} \begin{bmatrix} 1 & 0 & 0 \\ 0 & \cos\theta_1 & \sin\theta_1 \\ 0 & -\sin\theta_1 & \cos\theta_1 \end{bmatrix} \begin{bmatrix} \theta_1' \\ 0 \\ 0 \end{bmatrix}$$

We find, as expected,

$$M_x = +EI_x \theta_1' \tag{15}$$

Combining Equations 15 and 14, we have the differential equation for the elastica:

$$\theta_1'' - \frac{\mu g}{EI_x} (l - s) \sin\theta_1 - \frac{F_T}{EI_x} \cos\theta_1 = 0 \tag{16}$$

$$\theta_1(0) = \theta_1'(l) = 0$$

Equation 16 defines a nonlinear, two-point, boundary-value problem. When gravity is neglected ($\mu g = 0$) Equation 16 reduces to well-known differential equation for the elastica of a flexible beam and is solved in terms of elliptic functions[1].

The deflections $y(s)$, $z(s)$ follow from a further integration of the solution of Equation 16:

$$y(s) = \int_0^s -\sin\theta_1(\zeta)\, d\zeta \qquad z(s) = \int_0^s \cos\theta_1(\zeta)\, d\zeta$$

If we now assume θ_1 to be small, Equation 16 becomes a linear differential equation with variable coefficients of the polynomial type and a right-hand side

$$\theta_1'' - \frac{\mu g}{EI_x}(l - s)\,\theta_1 = + \frac{F_T}{EI_x} \tag{17}$$

The solution of the homogeneous part of this equation can be expressed in terms of the Bessel functions $J_{1/3}$ and $J_{-1/3}$, or Airy functions[5].

If we linearise also the expression for the curvature $\bar{\kappa} = -(\mathrm{d}^2 y)/\mathrm{d}z^2$, we obtain the following third-order differential equation for the deflection:

$$\frac{\mathrm{d}^3 y}{\mathrm{d}z^3} - \frac{\mu g}{EI_x}(l - z)\frac{\mathrm{d}y}{\mathrm{d}z} = -\frac{F_T}{EI_x} \tag{18}$$

The derivative of Equation 18 gives the fourth-order differential equation that would have been obtained with more traditional methods:

$$\frac{\mathrm{d}^4 y}{\mathrm{d}z^4} + \frac{\mu g}{EI_x}(l - z)\frac{\mathrm{d}^2 y}{\mathrm{d}z^2} - \frac{\mu g}{EI_x}\frac{\mathrm{d}y}{\mathrm{d}z} = 0 \tag{19}$$

Before discussing the solution of Equations 17 and 18, the differential equations corresponding to some other cases will be derived. The following remarks can made for this planar case:

- The components F_x, F_z of the inner force can be transformed into the normal stress and the shear stress via θ_1. It is an advantage of the method that the force components are introduced in the selected reference frame (not perpendicular to the cross-section), which simplifies the calculations.
- The condition $\theta_1'(l) = 0$ implies that measurements of the tip deflection angle are not critical with respect to the measurement point.

Linearised static deflections under a general tip load

Now we consider an applied tip load $\bar{F}_T = [F_{Tx}, F_{Ty}, F_{Tz}]$ in an arbitrary direction. The deflected centre line is no longer a planar curve and we linearise the rotation vector $\bar{\theta}$ from the outset: $\bar{\theta} = [\theta_1\ \theta_2\ \theta_3]^T$ and $\bar{\kappa} = \mathrm{d}\bar{\theta}/\mathrm{d}z$. The rotation matrix T needed for Equations 8 and 11 takes the form

$$T = E + A \tag{20}$$

where E is the unit matrix and

$$A = \begin{bmatrix} 0 & -\theta_3 & \theta_2 \\ \theta_3 & 0 & -\theta_1 \\ -\theta_2 & \theta_1 & 0 \end{bmatrix} \tag{21}$$

We again use Equation 9 and the boundary condition at the tip to produce

$$F_x(z) = F_{Tx} \qquad F_y(z) = F_{Ty} \qquad F_z(z) = \mu g\,(l - z) + F_{Tz} \tag{22}$$

To express Equation 10, the term $\mathrm{d}\bar{R}/\mathrm{d}s$ in the cross-product is written as given by the compatibility equation:

$$\frac{\mathrm{d}\bar{R}}{\mathrm{d}s} = \begin{bmatrix} \frac{\mathrm{d}x}{\mathrm{d}z} \\ \frac{\mathrm{d}y}{\mathrm{d}z} \\ 1 \end{bmatrix} = [E + A] \begin{bmatrix} 0 \\ 0 \\ 1 \end{bmatrix} = \begin{bmatrix} \theta_2 \\ -\theta_1 \\ 1 \end{bmatrix}$$

and we obtain

$$-M_x' + [\mu g(l - z) + F_{Tz}]\,\theta_1 + F_{Ty} = 0$$

$$-M_y' + [\mu g(l - z) + F_{Tz}]\,\theta_2 - F_{Tx} = 0$$

$$-M_z' - F_{Ty}\theta_1 - F_{Tx}\theta_1 = 0$$

The relation between M_i and θ_i follows from Equation 11:

$$\begin{bmatrix} M_x \\ M_y \\ M_z \end{bmatrix} = T \begin{bmatrix} EI_z & & \\ & EI_y & \\ & & GA \end{bmatrix} T^T \begin{bmatrix} \theta_1' \\ \theta_2' \\ \theta_3' \end{bmatrix}$$

To a first order, the above simply becomes

$$M_x = EI_x\,\theta_1' \qquad M_y = EI_y\,\theta_2' \qquad M_z = GA\,\theta_3'$$

and the differential equations for the θ_i read as follows:

$$EI_x\,\theta_1'' - \mu g\,(l - z)\,\theta_1 = +F_{Ty} \qquad \theta_1(0) = \theta_1'(l) = 0 \tag{23}$$

$$EI_y\,\theta_2'' - \mu g\,(l - z)\,\theta_2 = -F_{Tx} \qquad \theta_2(0) = \theta_2'(l) = 0 \tag{24}$$

$$GA\,\theta_3'' = -\{F_{Ty}\theta_2 + F_{Tx}\theta_1\} \qquad \theta_3(0) = \theta_3'(l) = 0 \tag{25}$$

The two bending equations in θ_1 and θ_2 are decoupled and reduce to the planar equation (16) if the tip load is horizontal ($F_{Tz} = 0$). Equation 25 shows how the torsion results from the solution of the bending equations. If $F_{Tx} = 0$, $\theta_2 = 0$ and the torsion remains zero, as it should for the planar deflections. Similarly, if $F_{Ty} = 0$, $\theta_1 = 0$ and so the torsion again remains zero.

Equations 23 and 24 can be converted into the equations for the displacements x, y by using $x' = \theta_2$, $y' = -\theta_1$ (compatibility equation).

Equations 23–25 may also be used to show that the torsion is zero for a symmetric cross section ($EI_x = EI_y = EI$). Writing the horizontal component of $\bar{F}_T$ in polar form,

$$F_{Tx} = F\cos\varphi \qquad F_{Ty} = F\sin\varphi$$

and defining

$$\Psi_1 = \theta_1\cos\varphi + \theta_2\sin\varphi$$

then Equation 23 × cos φ plus Equation 24 × sin φ produces

$$EI\Psi_1'' + [\mu g\,(l - z) + F_{Tz}]\,\Psi_1 = 0 \qquad \Psi_1(0) = \Psi_1'(l) = 0$$

Thus we find $\Psi_1 = 0$ as a solution and Equation 25 may be written

$$GA\,\theta_3'' = F\Psi_1 = 0 \qquad \theta_3(0) = \theta_3'(l) = 0$$

i.e. the solution is $\theta_3 = 0$, or no torsion.

For an asymmetric cross-section, the torsion following from Equation 25 will be small, as the right-hand side is a second-order quantity.

Planar vibrations

Although the only measurements envisaged on the axial antenna of ISPM were static deflections, it is interesting to derive the equations for the free vibrations. The availability of these equations can inspire different test measurements and also shows the capabilities of the method used.

To use the general equations for a problem of free vibration, all the vectors are considered as the sum of an equilibrium (subscript e) and a dynamic part (subscript d). The general equations are then split-up into equilibrium equations (applied forces present) and homogeneous linear dynamic equations, as, by definition, the free vibrations are about the equilibrium point. The example will illustrate this technique and more details can be found in Reference 3.

The equilibrium is trivial with zero deflections and inner moments:

$$\bar{F}_e = [0\,0\,\mu g\,(l - z)]^T \qquad \bar{R}_e = [0\,0\,z]^T \qquad \bar{M}_e = [0\,0\,0]^T$$

$$\bar{\kappa}_e = [0\,0\,0]^T \qquad \bar{\theta}_e = [0\,0\,0]^T$$

Considering only planar vibrations, we denote the dynamic variables as:

$$\bar{F}_d = [0 f_y\,0]^T \qquad \bar{R}_d = [0\,y\,0]^T \qquad \bar{M}_x = [m_z\,0\,0]^T$$

$$\bar{\kappa}_d = [\kappa_x\,0\,0]^T \qquad \bar{\theta}_d = [\theta_1\,0\,0]^T$$

Starting from Equation 2,

$$-\frac{\partial}{\partial s}(\bar{F}_e + \bar{F}_d) + \mu \frac{\mathrm{d}^2}{\mathrm{d}t^2}(\bar{R}_e + \bar{R}_d) = \mu g\,\bar{1}_z$$

we obtain equilibrium Equation 9 and the dynamic equation

$$-\frac{\partial F_d}{\partial s} + \mu \frac{\mathrm{d}^2 \bar{R}_d}{\mathrm{d}t^2} = 0 \tag{26}$$

For the planar vibrations, Equation 26 gives only one nonzero scalar equation:

$$-f_y' - \mu\omega^2 y = 0 \tag{27}$$

where the time derivative is replaced by $j\omega$.

The expansion of Equation 2 contains terms originating from the equilibri and gives the following dynamic equation

$$-\frac{\partial \bar{M}_d}{\partial z} - \frac{\partial \bar{R}_e}{\partial z} \times \bar{F}_d - \frac{\partial \bar{R}_d}{\partial z} \times \bar{F}_e = 0 \tag{28}$$

which gives one scalar equation:

$$M_x' + fy + \mu g\,(l - z)\,y' = 0 \tag{29}$$

The elastic equation and kinematic compatibility equation are simply $M_x = + EI_x \theta_1'$ and $\theta_1 = -y'$. Substitution in Equations 29 and 27 gives the following equation in y:

$$y^{IV} + \lambda_g^4[(1 - \zeta)y']' - \lambda^4 y = 0 \tag{30}$$

where

$$\lambda^4 = \frac{\mu\omega^2 l^4}{EI_x} \qquad \lambda_g^4 = \frac{\mu g l^3}{EI_x}$$

and the derivatives are with respect to the non-dimensional independent variable $\zeta = z/l$.

The frequency condition follows from the requirement of nontrivial solutions for the boundary conditions $y(0) = y'(0) = y''(1) = y'''(1) = 0$.

Solution of the differential equations

The solution of the equation describing the planar static deflections will be described here in some detail. Using this model, a first-order assessment of the two bending stiffnesses of the axial antenna is possible and predictions for the measured tip deflections have been calculated.

Rewriting Equation 17 in terms of the following nondimensional independent variable

$$\zeta = 1 - \frac{z}{l} \tag{31}$$

we find

$$\theta_1'' - a\zeta\theta_1 = -b \tag{32}$$

$$\theta_1(1) = \theta'(0) = 0$$

where

$$a = \frac{\mu g l^3}{EI_x}$$

$$b = \frac{F_T l^2}{EI_x}$$

Although a known set of independent solutions of Equation 32 are the Airy functions[5], which are related to the Bessel functions of order $\pm 1/3$, it is much more convenient to use directly the two base solutions $e_0(\zeta)$, $e_1(\zeta)$ of the homogeneous equation which satisfy the boundary conditions $e_0(0) = 1, e_0'(0) = 0, e_1(0) = 0, e_1'(0) = 1$. Assuming that the $e_i(\zeta)$ have a series representation $e_i = \Sigma_0\, c_k\, \zeta^k$, one finds easily that the c_k satisfy the recurrence relations

$$c_{k+3} = a\frac{c_k}{(k+2)(k+3)} \tag{33}$$

and start respectively with $c_0 = 1, c_1 = c_2 = 0$ for e_0 and $c_0 = 0, c_1 = 1, c_2 = 0$ for e_1. They can also be denoted by

$$e_0(\zeta) = f(\sqrt[3]{a}\,\zeta) \quad e_1(\zeta) = \frac{1}{\sqrt[3]{a}}\, g(\sqrt[3]{a}\,\zeta) \tag{34}$$

where

$$f(x) = 1 + \frac{x^3}{3!} + 4\frac{x^6}{6!} + 4.7\frac{x^9}{9!} + \ldots. \tag{35}$$

$$g(x) = x + 2\frac{x^4}{4!} + 2.5\frac{x^7}{7!} + 2.5.8\frac{x^{10}}{10!} + \ldots. \tag{36}$$

We also need a particular solution corresponding to a constant right-hand side. As a fundamental set of solutions of the homogeneous equation is known, it is always

possible to construct a particular solution with the general method of variation of parameters.

The calculations are much simplified if we exploit the fact that the right-hand side is simply a constant by assuming a power series solution similar to the e_i. One finds the same recurrence relation (33) for the coefficients and the starting values are $c_0 = c_1 = 0, c_2 = -b/2$.

If we denote the particular solution as P, then

$$P(\zeta) = -\frac{b}{(3a)^{2/3}} h(\sqrt[3]{3a}\,\zeta)$$

where

$$h(x) = \frac{x^2}{2!} + 1!\frac{x^5}{5!} + 2!\frac{x^8}{8!} + 3!\frac{x^{11}}{11!} \tag{37}$$

Now the general solution to Equation 32 is

$$\theta_1(\zeta) = A\,e_0(\zeta) + B\,e_1(\zeta) + P(\zeta) \tag{38}$$

$$\theta_1(1) = \theta_1'(0) = 0$$

Using the boundary conditions to identify A and B,

$$\theta_1(\zeta) = -\frac{P(1)}{e_0(1)} e_0(\zeta) + P(\zeta) \tag{39}$$

Hence, only one of the base functions is required. The tip-deflection angle $\theta_1(0)$ is given by

$$\theta_1(0) = -\frac{P(1)}{e_0(1)} = \frac{b}{(3a)^{2/3}} \frac{h(\sqrt[3]{3a})}{f(\sqrt[3]{a})} \tag{40}$$

By integrating $\theta_1(\zeta)$, one obtains similar expressions for the linear tip displacements:

$$y_{tip} = l \int_0^1 -\theta_1(\zeta)\,\mathrm{d}\zeta$$

or

$$y_{tip} = \frac{b \cdot l}{(3a)^{2/3}} \left\{ \frac{h(\sqrt[3]{3a})}{e_0(1)} \int_0^1 e_0(\zeta)\,\mathrm{d}\zeta - \int_0^1 h(\sqrt[3]{3a}\,\zeta)\mathrm{d}\zeta \right\} \tag{41}$$

which, after some calculations can be computed from

$$y_{tip} = b \cdot l \left\{ \frac{h(\sqrt[3]{a})}{f(\sqrt[3]{a})} F_2(a) - H_2(a) \right\} \tag{42}$$

where H_2, F_2 satisfy recurrence relations obtained by integrating h and f term by term, and we have

$$H_2(a) = \frac{1}{3!} + \frac{3a}{6!} + 2!\frac{(3a)^2}{9!} + 3!\frac{(3a)^3}{12!} \tag{43}$$

$$c_0 = \frac{1}{6} \qquad c_n = a c_{n-1} \frac{3n}{(3n+1)(3n+2)(3n+3)} \qquad n \geq 1$$

$$F_2(a) = 1 + \frac{a}{4!} + 4\frac{a^2}{7!} + 4.7\frac{a^3}{10!} + \ldots.$$

$$c_0 = 1 \qquad c_n = a\, c_{n-1} \frac{3n-2}{(3n-1)\,3n\,(3n+1)} \qquad n \geq 1 \tag{44}$$

From Equations 40 and 42 one can prepare the two curves, shown in Figures 3 and 4, that show the linear and angular tip deflection per unit gram lateral load as a function of the bending stiffness. Both curves are calculated for an antenna length of 8 m and a linear density $\mu = 0.034$ kg/m. The dashed lines indicate the bending stiffnesses obtained from earlier tests with gravity compensation.

It is interesting to compare these results with the solution without gravity. Under this assumption, $a = 0$ and Equation 32 reduces to

$$\theta_1'' = \frac{F_T l^2}{EI_x} \qquad \theta_1'(0) = \theta_1(1) = 0 \tag{45}$$

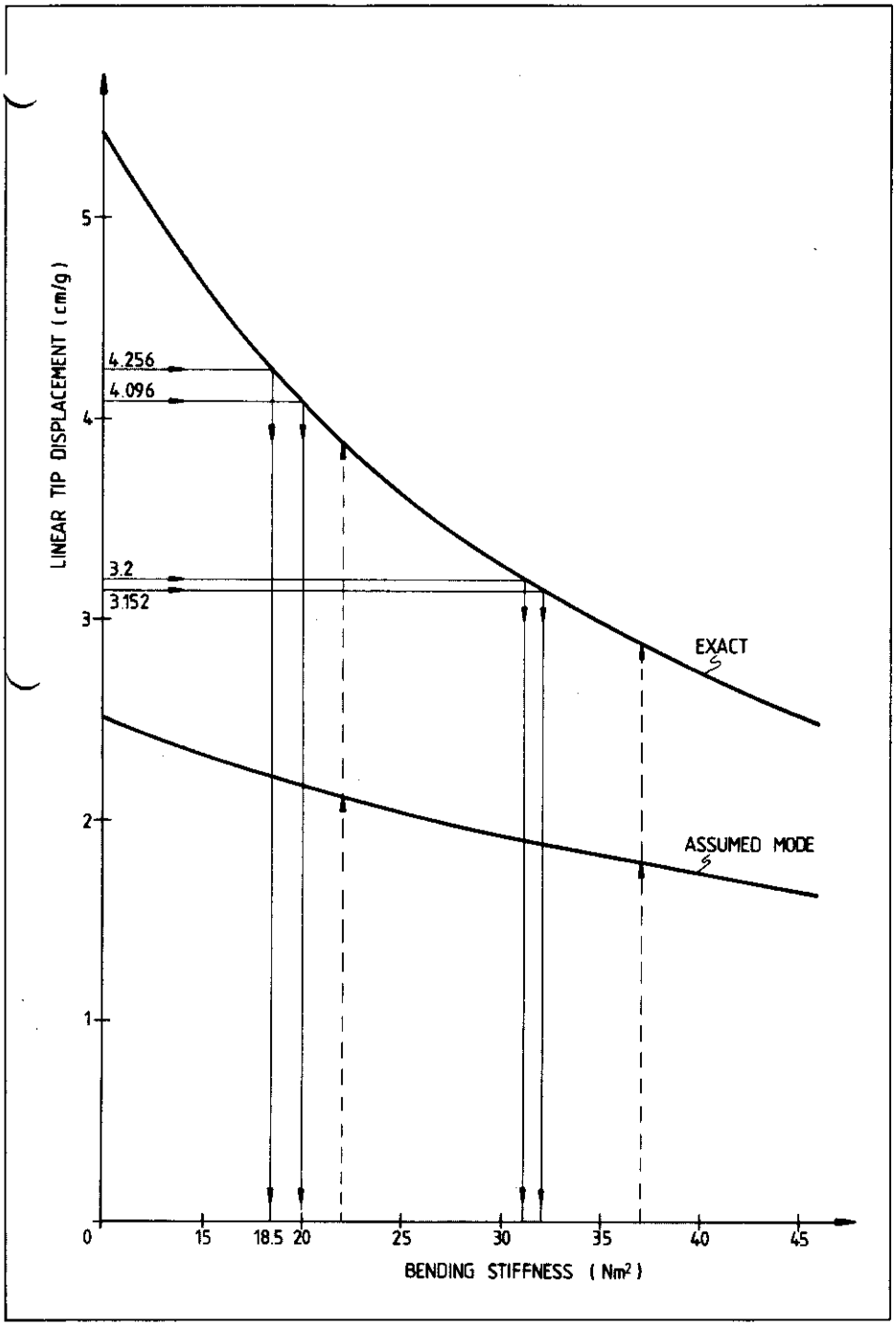

Figure 3. Linear tip displacement per unit gram lateral load (cm/g) as a function of bending stiffness (Nm^2) [$l = 8$ m, $\mu = 0.034$ kg/m]

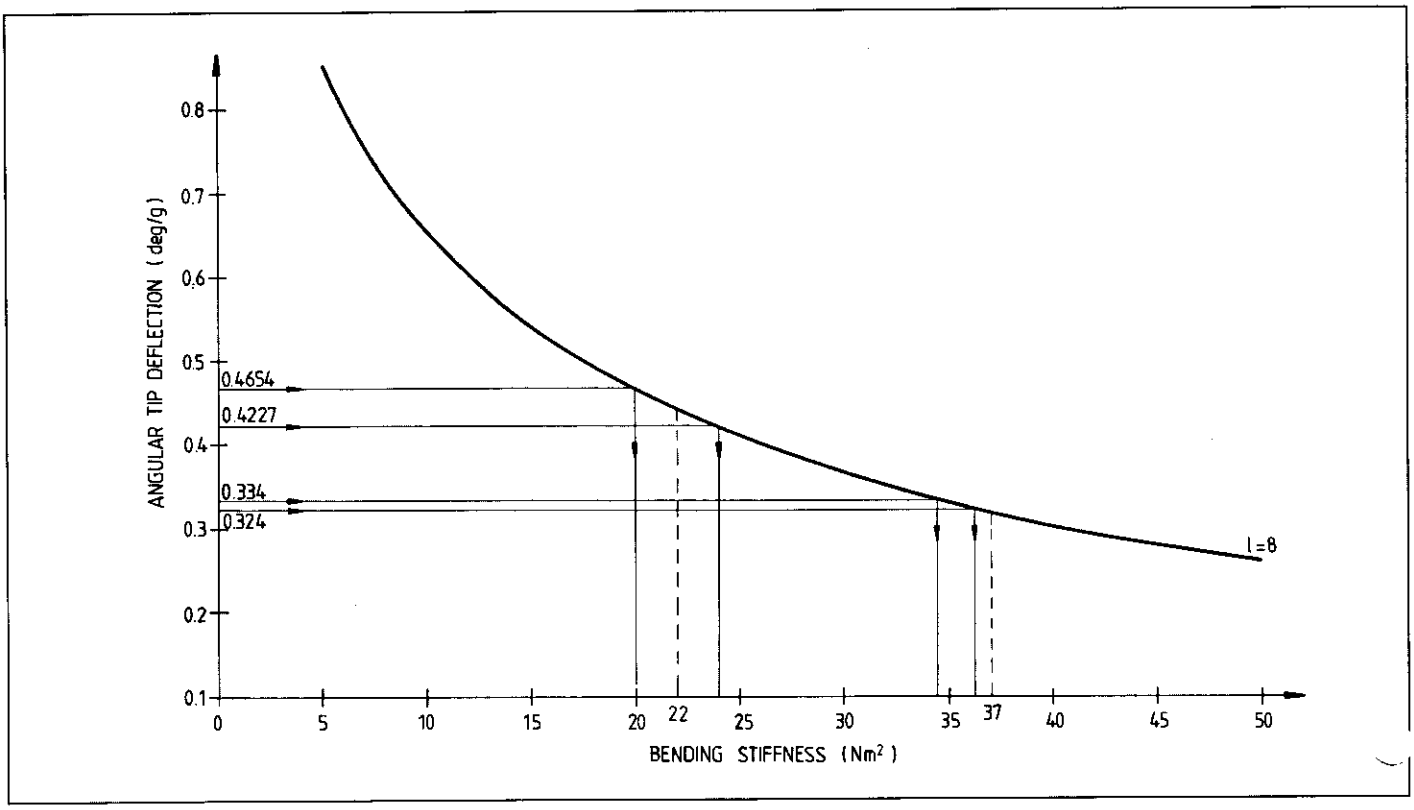

Figure 4. Angular tip deflection per unit gram lateral load (deg/g) as a function of radial stiffness (Nm^2) [$l = 8$ m, $\mu = 0.034$ kg/m]

The solution of Equation 45 is

$$\theta_1(\zeta) = \frac{F_T l^2}{2EI_x}(\zeta^2 - 1) \rightarrow [\theta_1(0)]_{w.g.} = -\frac{F_T l^2}{2EI_x} \tag{46}$$

which could also be obtained by evaluating Equation 40 for $a = 0$.

For the tip deflection y_T one obtains in the same way

$$[y_T]_{w.g.} = \frac{F_T l^3}{3EI_x} \tag{47}$$

Neglecting gravity, the curves of Figures 3 and 4 are replaced by two hyperbolas. The same hyperbolas appear as a factor (term b) in Equations 40 and 42 and the remainder of these equations can be interpreted as a correction factor depending only on the ratio of the gravity forces to the flexibility $[a = (\mu l)\, g l^2/EI_x]$.

Figure 3 contains a second curve (assumed modes), proposed in Reference 6, based on the formula

$$[y_T]_{a.m.} = \frac{F_T l^3}{3EI_x}\,\frac{1}{1 + \frac{a}{3}} \tag{48}$$

The correction factor in Equation 48, when compared to Equation 47, has been obtained by assuming that the shape of the deflections is still the third-order polynomial corresponding to the zero-gravity solution and modelling the gravity as a concentrated load. The figure shows that the results are wrong by a factor of approximately 2.

Later in Reference 6 another solution is proposed based on a discretisation procedure and using a finite-element model (an 8-element model was used). The results are identical for bending stiffnesses above 25 Nm^2, but deviate increasingly for lower bending stiffnesses. A priori, one would indeed expect that the more flexible the beam, the finer the discretisation that is needed.

The solutions to Equations 23 and 24 and Equation 30 can be obtained by the

same methods as used in this section. For interpretation of the test results, Equations 40 and 42 are the more important.

Test description and results

During the tests, the ISPM antenna was hung fully deployed (8.0 m) from its stowage/deployment unit, which it leaves via two guide rollers (modelled as a clamped root). Four plumb lines were attached to the deployment unit in such a way that they defined a set of reference axes for the measurements.

The origin of the axis set was on the antenna centre line at the root. The x-axis was aligned with the weaker principal bending direction of the cross-section at the root and the y-axis with the stronger. This axis set was transferred to the tip of the antenna via the plumb lines. The natural (unstressed) tip offsets were found to be 3.6 cm in the x-direction and 1.7 cm in the y-direction. The natural twist of the cross-section was 11.5°. The definition of the reference axes was such that the parallelism of the x- and y-axis with the principal bending directions at the root was more precise than the location of the centre line. The measurement of the natural twist over the antenna's length is therefore more precise than that of the natural tip offset.

The antenna was loaded horizontally at the tip with a small weight of ~6 or ~12 g via a pulley and a tripod (Fig. 5). It must be noted that, in the deflected state, second-order effects change the direction of the applied load (horizontally as well as vertically) due to the finite distance to the tripod, and also the magnitude of the applied load (friction in the pulley). These effects were not measured in the test. In the deflected state, the three components of the angular deflection at the tip were measured directly using a cubic mirror glued to the tip and two theodolites. The linear displacements, measured on graph paper, were repeated for loads of 6.5 and 12.75 g in steps of 45° in a horizontal plane. More detailed information on the test set-up is given in Reference 6.

Tables 1 and 2 give the measurements along the principal bending directions at the tip. To eliminate the uncertainty in the neutral position of the antenna, only

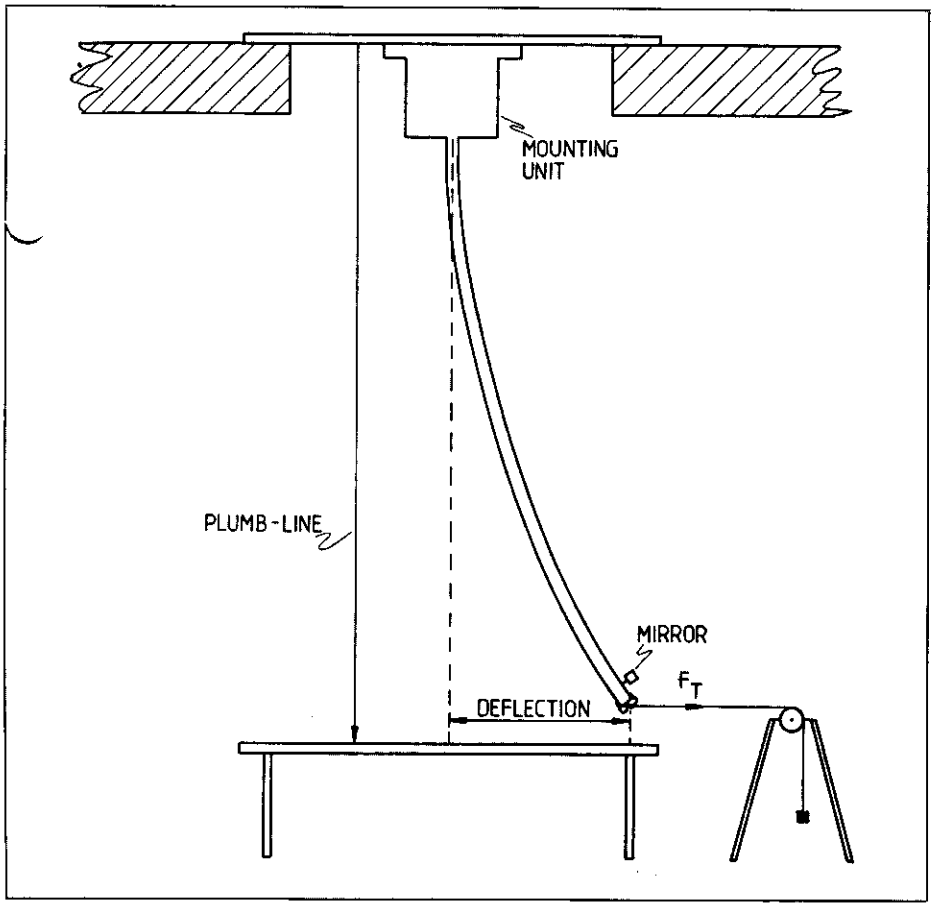

Figure 5. Test-arrangement schematic

the differences in deflections due to the two loads are converted into bending stiffnesses. This approach is always valid for cases in which a linear relationship exists between forces and displacements.

The difference in stiffness between the + and -- directions provides an indication of the uncertainty in the result. As this uncertainty results from a large number of error sources, the average stiffness is taken as the final estimate. The linear tip displacements give systematically lower estimates than the angular deflections, which are considered to be more precise. The results of the angular measurements are in better agreement with the estimates derived from the floating antenna.

Table 1. Angular measurements

	Angular deflection (°)				EI	
	6.6 g	12.75 g	Δ = 6.25 g	deg/g	(Nm^2)	$\overline{EI}$
+X	2.59611	5.3986	2.6422	0.42275	24	22.25
--X	2.27416	5.18833	2.9086	0.46538	20.5	
+Y	2.19333	4.21666	2.0233	0.32373	36.4	35.4
--Y	1.75499	3.84333	2.0883	0.33413	34.4	

Table 2. Tip displacements

	Tip displacement (cm)				EI	
	6.5 g	12.75 g	Δ = 6.25 g	cm/g	(Nm^2)	$\overline{EI}$
+X	22.4	49	26.6	4.256	18.5	19.25
--X	22.0	47.6	25.6	4.096	20	
+Y	17	37	20	3.2	31.2	31.6
-Y	20	39.7	19.7	3.152	32	

Conclusion

The equations describing the static deflections of a flexible beam under a distributed load due to gravity and a concentrated tip load have been derived by a general vectorial method. The linear differential equations with variable coefficients have been solved to obtain predictions for these deflections. The results show that, in spite of the small mass of the flexible antenna, gravity must be modelled as a distributed load in order to obtain sensible results.

The results of the analysis have been used to interpret the measurements fr the static deflection tests on the ISPM spacecraft's antenna. The results obtained via the angular deflections at the tip agree best with the results of earlier tests with gravity compensation.

References

1. Love A E H 1952. The Mathematical Theory of Elasticity. Cambridge University Press
2. Landau L & Lifschitz E 1967. Elasticité Editions Mir, Moscou
3. Janssens F & Kulla P. Vibrations of flexible beams on a rotating base. Submitted for publication in *AIAA J*
4. Leigh D C 1968. Nonlinear Continuum Mechanics. McGraw-Hill
5. Abramowitz M 1970. Handbook of Mathematical Functions. Dover Publications.
6. Axial boom stiffness measurements. ISPM Test Report Doc. No.: IS-TR-DS-3076/C1, April 1983.

Manuscript received 29 April 1983